RSC Advances

ROYAL SOCIETY OF CHEMISTRY

www.rsc.org/advances

Polyelectrolyte-modified layered double hydroxide nanocontainers as vehicles for combined inhibitors

Jorge Carneiro[1], Ana F. Caetano[1], Alena Kuznetsova[1], Frederico Maia[1], Andrei N. Salak[1], João Tedim[1*], Nico Scharnagl[2], Mikhail L. Zheludkevich[1,2], Mário G.S. Ferreira[1]

[1]Department of Materials and Ceramic Engineering, CICECO-Aveiro Institute of Materials, University of Aveiro, 3810-193 Aveiro, Portugal

[2]Helmholtz-Zentrum Geesthacht Centre for Materials and Coastal Research GmbH Institute of Materials Research - MagIC, Max-Planck-Strasse 1, 21502 Geesthacht, Germany

(*) **Corresponding author:** J. Tedim, joao.tedim@ua.pt Universidade de Aveiro, CICECO, Dept. Engenharia de Materiais e Cerâmica, 3810-193, Aveiro, Portugal, tel. (+351)234370255

Abstract. In this work, nanocontainers based on layered double hydroxide (LDH) loaded with two different corrosion inhibitors, namely 2-mercaptobenzothiazole (MBT) and cerium (III) nitrate, were prepared. MBT was intercalated into LDH galleries in anionic form by anion-exchange, while Ce^{3+} was fixed between polyelectrolyte layers on the surface of LDH-MBT nanoplatelets by the Layer-by-Layer (LbL) method. Both inhibitors were found in the modified LDHs (LDH-Mod) by X-ray diffraction and Scanning Electron Microscopy coupled with Energy Dispersive Spectroscopy. The release studies performed by UV-Vis spectrophotometry indicated that the main triggering conditions for release of MBT from LDHs changed when LDH nanoplatelets were covered with polyelectrolytes. Furthermore, Electrochemical Impedance spectroscopy and DC polarization were used to investigate the effect in combining MBT^- and Ce^{3+} within the same nanocontainer, for the corrosion protection of 2024-T3 aluminium alloy directly in solution as well as in a hybrid sol-gel coating. The obtained results open prospects for application of these systems as additives in multifunctional smart coatings.

Keywords: LDH nanocontainer; polyelectrolyte; active corrosion protection; dual-release.

1. Introduction

In the last decade much attention has been devoted to development of self-healing coatings based on controlled release of corrosion inhibitors. The use of containers capable of storing corrosion inhibitors has been studied as a suitable alternative to the direct addition of corrosion inhibitors. Encapsulation in particular can provide several advantages: limit spontaneous leaching of inhibitor from the coating into the environment, avoid detrimental interactions between coating matrix and inhibitor and release the corrosion inhibitor on demand (so called "smart" release). Several systems have been used as containers for corrosion inhibitors: polyurethane microcapsules,[1] silica-based nanoparticles and nanocapsules,[2-5] halloysites[6-8] and layered double hydroxides (LDHs).[9-14]

Layered doubled hydroxides are hydrotalcite-like structures composed by positively-charged, mixed-metal hydroxide layers (typically M(II)-M(III)), intercalated with anions and water molecules.[15] From the wide range of containers reported so far, LDHs are among the most promising systems. Several studies present LDHs as versatile reservoirs for corrosion protection, showing good efficiency when loaded with 2-mercaptobenzothialzole (MBT),[12] 2-benzothiazolylthio-succinic acid,[10] tungstate[11] and vanadate ions.[13] Furthermore, the use of LDHs has not been restricted to application as "smart" reservoirs, but also as nanostructured layers directly grown on the surface of the metallic substrates. Since the pioneering works of Buchheit and colleagues,[16-18] other groups have worked on development of LDH conversion films to render protection to the underlying substrate. These include the preparation of LDH layers with superhydrophobic properties,[19] LDHs intercalated with carbonates to decrease anion-exchange capability[20] and works by our group on the intercalation and controlled release of corrosion inhibitors.[21, 22]

Recently, the first study on the positive effect of combining different corrosion inhibitors within layered double hydroxides nanoreservoirs for protection of 2024 aluminium alloy

(AA2024) was reported.[23] Among possible difficulties and challenges for development of coating formulations with nanocontainers, the loading content and the diffusivity of species in sufficient amounts to act on a defect was highlighted.[23] In this context, the combination of corrosion inhibitors can assume a prime role to circumvent these limitations, particularly relevant for alloys where the galvanic coupling between metals can be the main cause of corrosion.

Forsyth and co-workers reported studies on combination of rare earth metallic element with a multifunctional organic component to achieve synergistic corrosion protection of AA2024.[24, 25] Recently, Kallip and co-workers reported the synergistic inhibition of galvanically coupled Ze+Fe metals, when 1,2,3-benzotriazole and $Ce(NO_3)_3$ were combined.[26]

One topic that has not yet been covered in detail is the co-intercalation of different corrosion inhibitors within the same carrier. The incorporation of MBT in cerium molybdate hollow nanospheres were found to render corrosion protection to galvanized steel substrates when combined in coatings with LDH-MBT.[12] In this case, authors suggested that the inhibiting effect could be associated with MBT, as well as to dissolution of cerium and molybdate ions from the nanospheres under acidic conditions. Very recently, Ferrer and co-workers reported the preparation of NaY zeolites with cerium and diethyldithiocarbamate corrosion inhibitors, investigating the effect of this double-doped zeolite for corrosion protection of AA2024 alloy.[27] Positive results were obtained with the zeolites in solution and when added to sol-gel coatings. Apart from these works, not much has been done in the co-intercalation of corrosion inhibitors.

In this paper we go beyond mono-, towards multi-intercalation and release of corrosion inhibitors in a controlled manner (Scheme 1). The strategy followed consists of using a system well known for its intrinsic controlled release mechanism (LDHs), modifying its

surface with polyelectrolytes by the Layer-by-Layer (LbL) technique. The use of polyelectrolytes allows the intercalation of additional corrosion inhibitors between layers, which can be released due to pH-dependent permeability of polyelectrolytes.[28, 29]

The objective of this work is to investigate Zn-Al LDHs as containers for two corrosion inhibitors simultaneously. 2-mercaptobenthiazole (MBT), a well-known corrosion inhibitor for AA2024,[30] was intercalated in interlayer of the LDH structure by ion-exchange according to a procedure described in the literature[31], while Ce^{3+}, also known as an effective corrosion inhibitor for AA2024,[32] was adsorbed between polyelectrolyte layers on the surface of **LDH-MBT** platelets. The modified LDH particles (**LDH-Mod**) were characterized by X-ray Diffraction (XRD) and Scanning Electron Microscopy with Energy-dispersive X-ray Spectroscopy (SEM-EDS). Furthermore, the influence of LDH surface modification in the release of MBT was investigated by UV-Visible Spectrophotometry and correlated with electrochemical studies by DC polarization and Electrochemical Impedance Spectroscopy (EIS), in solution and as additives to a hybrid sol-gel coating.

Scheme 1

2. Experimental

2.1. Materials. All the chemicals were obtained from Aldrich, Fluka, and Riedel-de Haen, with ≥98% of ground substance, and used as received. AA2024-T3 with the following composition was used: Cu 3.8-4.9 %, Mg 1.2-1.8 %, Mn 0.3-0.9 %, Fe 0.5 %, Si 0.5 %, Zn 0.25%, Ti 0.15 %, Cr 0.1 %, other 0.15 %, balance Al. All the alloy panels were chemically etched prior to coating applications by a two-step cleaning procedure. Firstly, the panels were immersed in a 2 wt. % solution of a commercial cleaning product (Gardacid® P 4307 from Chemetall) at room temperature for two periods of 45 seconds, with an intermediate washing

step in distilled water. Then, panels were subjected to acid etching in a Turco Liquid Smutgo NC (Turco Chemie GmbH) at 30 ± 5 °C for 5-10 min. After chemical etching, all the metallic panels were thoroughly washed with distilled water and left to dry at room temperature.

2.2. LDH synthesis and intercalation of MBT. LDH synthesis was described in previous works reported by our group.[31, 33] A solution prepared by dissolution of $Zn(NO_3)_2.6H_2O$ and $Al(NO_3)_3.9H_2O$ (0.5 M/0.25 M) was added to 1.5 M $NaNO_3$ under vigorous stirring at room temperature. To avoid contamination with carbonate all solutions were prepared using boiled distilled water and the synthesis was carried out under nitrogen atmosphere. The pH was fixed (pH =10±0.5) and controlled by simultaneous addition of a 2 M NaOH solution. The final suspension was subjected to hydrothermal treatment at 100 ºC during 4 h for crystallization of the LDH material. In the end, the obtained slurry was centrifuged and washed four times with boiled distilled water.

For the ion-exchange reaction, 0.1 M of MBT solution (pH=9) was prepared. LDH-NO_3 was added to the inhibitor containing solution and left under stirring for 24 hours. After centrifugation and washing steps (2 times), the procedure was repeated with a second portion of MBT solution to guarantee a complete exchange of NO_3^- with MBT. In the end, the reaction products were isolated by centrifugation and washed 2-4 times with boiled distilled water to ensure that all MBT in excess was removed. The washed yellowish LDH deposit was consequently stored at room temperature in sealed plastic reservoirs, to maintain the water content and avoid contamination with carbonates from atmosphere.

2.3. Surface modification of LDHs. The modification of LDHs was carried out by the LbL method, with addition of cerium (III) nitrate during the deposition process, using negatively-charged poly(sodium styrene sulfonate) (PSS) and positively-charged poly(allylamine hydrochloride) (PAH) polyelectrolytes. In the first step, an aqueous LDH slurry (0.5 g of dry content) was added to 0.5 wt. % of PSS solution in deionized water.

Thereafter, the slurry was dispersed with magnetic stirring (10 min) and ultrasound treatment (10 min). After complete dispersion the suspension was left under magnetic stirring for 20 min. Finally, LDHs were recovered by centrifugation, followed by 3 consecutive washing/centrifugation stages to remove PSS in excess.

In the second step, the LDH particles were re-dispersed in a 0.1 M cerium (III) nitrate solution and left for one day under stirring at room temperature. Then, LDHs were recovered by centrifugation and washed/centrifuged 3 times with distilled water. In the third step, a second layer of PSS was deposited after treatment with cerium solution, following the same procedure used in the first deposition, to ensure that cerium incorporation was not reversible and to prepare the surface for the subsequent positive polyelectrolyte. The final layer of PAH was applied using similar conditions of concentration and time applied for PSS. The modified LDH was kept as a water-based slurry in a sealed container.

2.4. Coating preparation. The active corrosion protection conferred by LDHs was evaluated directly in solution and using LDHs as additives in a hybrid-based sol-gel coating. The hybrid-based coating was prepared by a controllable hydrolysis of metalorganic titanium (IV) propoxide (TPOT) and 3-glycidoxypropyltrimethoxysilane (GPTMS), phenyl trimethoxysilane (PTMS) and hexadecyltrimethoxysilane (HDTMS) under acidic conditions.[34] The first sol was obtained by mixing the TPOT solution, formed by mixing the precursor (70 wt.% in 2-propanol) with 2-propanol in a 2.5:1 weight ratio, with acetylacetone in 2:1 volume ratio during 20 min. Afterwards, the solution was hydrolysed during 1 h in the presence of 0.32 M HNO_3 aqueous solution with molar ratio 3:1 of acidified water to TPOT. The second solution was obtained by mixing GPTMS, PTMS and HDTMS in 1:1:0.15 volume ratio. The solution was hydrolysed by adding 0.1 M HNO_3 in 4:1 molar ratio of water to GPTMS under constant mechanical stirring during 1 hour. Consequently, the two solutions were mixed and left at 22±1ºC under constant stirring for 1 hour. In the end, the LDH

particles were added to the formulation (0.5 wt. % with respect to the total formulation) and stirred until obtaining a uniform dispersion (~10 minutes). The AA2024 samples were dipped into the sol-gel formulations at 18 cm/min and immersed during 90 seconds followed by withdrawal at 18 cm/min. The coatings were cured using the following procedure: after deposition the samples left in contact with air during 20-30 min at room temperature and then transferred to an oven pre-heated at 60 ºC and held at this temperature for 10 min. The samples were heated at a rate of 4 ºC/min until maximum temperature of 120 ºC, where was kept for 80 min. Consequently, the coated samples were removed from oven.

2.5. Release studies. The release of MBT from LDHs was performed under stirring conditions at room temperature, under the following conditions: 50 mM NaCl, pH=11 and pH=4. Three replicas were obtained for all the conditions investigated (standard deviation was lower than 3%). UV-Vis measurements were performed following the same timescale for all the samples: 0 min, 30 min, 1 h, 2 h, 3 h, and 4 h. The total amount of MBT intercalated in LDHs was determined by complete dissolution of LDHs into 0.1 M HNO_3, followed by UV-Vis measurement of MBT in solution.

2.6. Characterization methods. X-ray diffraction (XRD) analysis was performed using a PANalytical XPert MPD PRO diffractometer (Ni-filtered Cu$K\alpha$ radiation, PIXEL 1D detector, and the exposition corresponded to about 2 s per step of 0.02^{o} at room temperature). LDHs were characterized by XRD as dried powders.

Thermogravimetric analysis (TGA) was performed using a Setaram SetSys 16/18 instrument between room temperature and 1000°C with a heating rate of 1°C/min in air.

SEM/EDS analysis was performed using a Hitachi S-4100. The EDS mapping was performed in a Hitachi SU-70 microscope with electron beam energy of 25 kV for EDS and 15 kV for SEM micrographs.

X-ray photoelectron spectroscopy (XPS) was carried out by using a Kratos DLD Ultra Spectrometer with an Al-Kα X-ray source (monochromator) operated at 225 W. For the survey spectra a pass-energy (PE) of 160 eV was used while for the region scans PE was 40 eV. Spectra were calibrated to 284.8 eV binding energy of C1s signal. For all samples charge neutralization was necessary. With respect to deconvolution of the region files background subtraction (linear or Shirley) was performed before calculation. Smoothing was necessary for quantitative calculations on the Ce(3d) core region.

The release of MBT was studied using an UV-Vis spectrophotometer (Scanspec UV-Vis) at 320 nm wavelength. Particle zeta potential was assessed using a Zetasizer Nano ZS, performed by the combination of laser Doppler velocimetry and phase analysis light scattering (PALS) in a Malvern's patented M3-PALS technique.

DC polarization technique was employed to study MBT and cerium salt corrosion inhibition properties for bare AA2024.[30, 35] The DC polarization curves were obtained using a Gamry potentiostat PCI4. The potential was scanned with a sweep rate of 1 mVs^{-1} in the range of -1.2 to -0.3 V vs. SCE. The OCP was stabilized for 1 h and 24 h prior to the beginning of measurements. A three-electrode cell, consisting of abraded AA2024 (chemical etched as described above) with an area of 1 cm^2 (working electrode), Pt spring with total surface area of 2 cm^2 (counter electrode) and a saturated calomel electrode (reference) combined with the Luggin capillary, was used.

Electrochemical impedance spectroscopy (EIS) was used to evaluate the protective performance of LDH additives (coatings) against corrosion of aluminium alloy in a 50 mM (500 mM) NaCl aqueous solution. The measurements were carried out with a Gamry FAS2 Femtostat coupled with a PCI4 controller at open circuit potential with an applied 10 mV sinusoidal perturbation in the 100 kHz to 10 mHz frequency range, taking 7 points per decade. For this purpose, a conventional three-electrode cell was used, composed of a

saturated calomel reference electrode, a platinum foil as the counter electrode, and uncoated (coated) AA2024 substrates as the working electrodes, with a surface area of 3.3 cm^2.

3. Results and Discussion

3.1 LDH characterization. XRD patterns of the as-prepared samples of LDH-NO_3 (by direct synthesis) and LDH-MBT (by anion exchange from the respective nitrate) are shown in Figure 1. LDH-NO_3 was identified as a single-phase layered double hydroxide. The basal plane spacing (*d*) value was calculated from positions of the fundamental reflections (00*l*) to be 0.90 nm which is consistent with the respective reported data for Zn-Al LDHs intercalated with NO_3^-.[31, 33]. XRD pattern of Zn-Al-MBT (labelled hereafter as **LDH-MBT**) obtained through ion-exchange from the parent LDH-nitrate is similar to that previously reported.[31] Specifically, two LDH phases with the *d*-values of 1.67 and 0.76 nm were detected. These phases correspond to LDHs intercalated with either MBT^- or OH^- anion. The molar ratio of the LDH-OH phase in the obtained **LDH-MBT** powder was found to be about 15%. No shift in position of the (110) reflection peak for both the parent LDH-nitrate and **LDH-MBT** was observed (see inset in Figure 1) indicating that the ion exchange 'nitrate-to-MBT' has not affected the cation composition of the hydroxide layers.

Chemical structure of LDHs is represented by the generic formula $[M^{2+}_{1-x}M^{3+}_{x}(OH)_2]^{x+}\ A^{z-}_{x/z}\cdot nH_2O$, where $M^{2+}$and M^{3+} are the bi- and trivalent metal cations, A^{z-} is the intercalated anion and *n* is the molar fraction of crystal water.[36-38] Chemical compositions of the as-prepared LDH-NO_3 and LDH-MBT were refined using an approach based on joint analysis of TGA and XRD data.[39] The powder calcined at 1000^{o}C as a result of TGA experiment was studied by XRD. The calcination resulted in a complete deconstruction of the LDH structure and formation of two well-crystallized phases: ZnO and $ZnAl_2O_4$. The relative amounts of each phase in the mixture were estimated from the Rietveld analysis of the XRD data. Then

the Zn/Al ratio in the calcined powder (and thereby, in the initial LDH sample) was calculated to be 1.9. The relative amounts of crystal water in LDHs were roughly estimated from the TGA weight loss between room temperature and 200°C. The obtained data allowed us to estimate the chemical structures of the as-prepared LDH-nitrate and **LDH-MBT** as the following: $[Zn_{0.66}Al_{0.34}(OH)_2](NO_3)_{0.34}\cdot n_1H_2O$ and $[Zn_{0.66}Al_{0.34}(OH)_2]MBT_{0.34}\cdot n_2H_2O$, respectively, with n_1=0.3-0.4 and n_2=0.4-0.5.

The subsequent treatments (modifications) of **LDH-MBT** were found to result in appearance of LDH phases with *d*-values different from those characteristic of either LDH-MBT or LDH-OH (Figure 1). More specifically, an additional LDH phase with *d*~1.97 nm was detected in the sample after the first modification step with PSS (**LDH_P(-)**). This can be caused by re-arrangement of MBT^- under the experimental conditions or result from a (partial) anion-exchange of MBT^- and OH^- with charged species available in the PSS solution. After the second modification step (immersion in a cerium (III) nitrate solution, **LDH_P(-)_Ce**), the XRD patterns exhibit additional reflections at 28.8, 33.1, 47.5 and 56.3º (Figure 1), indicating the occurrence of a crystalline phase of cerium (IV) oxide.[40-42] The symmetric broadening of these reflections suggested that the CeO_2 crystallites are nano-sized. More importantly, the main LDH phase in the sample after treatment in $Ce(NO_3)_3$ solution (*d*~0.90 nm) is consistent with a Zn(2)-Al-NO_3 LDH,[43] whereas the relative amount of LDH-MBT (1.67 nm) was estimated to be *only about 10%* of the starting LDH-MBT phase, before the LbL procedure. The XRD pattern after the third modification stage with PSS (**LDH_P(-)_Ce_P(-)**) is similar to the pattern after first stage (both are carried out in a PSS solution). The main difference is that **LDH_P(-)_Ce_P(-)** contains less amount of LDH-MBT phase than **LDH_P(-)**.

The fourth stage (treatment in a PAH solution, **LDH-Mod**) resulted in some changes in the basal spacing values of both phases (from 1.97 and 1.67 nm to 1.90 and 1.09 nm, respectively) and disappearance of the LDH-OH phase.

The main point to highlight at this stage is that, being LDHs anion-exchangers, any species prone to be exchanged could compete for intercalation. It seems that during the LbL process 90% of the LDH-MBT initially existing in the unmodified LDH disappeared, while the amount of crystalline cerium (IV) oxide after the second stage remained constant.

Figure 1

A doubt raised by the XRD analysis of modified LDHs was whether all the cerium incorporated by the LbL process is in the form of nano-sized CeO_2 or if a fraction was kept as Ce^{3+}. In order to reveal any "hidden" cerium from a structural point of view, the relative metal cations ratio was estimated from XRD analysis of LDH powder calcined at 1000^{o}C for 6 h in air as described above. Three crystalline phases, namely ZnO, $ZnAl_2O_4$, and CeO_2 were found in the calcined **LDH_P(-)_Ce** (Figure 2). The relative amounts of each phase in the mixture were calculated to be 48.7, 39.5 and 11.9 wt. %, respectively. The ratios of metal cations were then calculated to be the following: Zn/Al=1.9 and Zn/Ce=11.9. Provided that all cerium in the sample is in a form of crystalline Ce(IV) oxide, the latter would correspond to the weight ratio of Zn(2)-Al-MBT LDH to CeO_2 of about 17. For comparison purposes, powders of the as-prepared LDH-MBT were mixed with CeO_2 nano-particles synthesized according to reference [42] in the aforementioned proportion, milled in a mortar, and studied by XRD (Figure 2). The intensities of reflections corresponding to cerium (IV) oxide in the XRD pattern of the modified LDH-MBT sample after the second stage is regularly smaller than the respective intensities in the XRD pattern of the mechanical mixture "LDH-MBT +

nano-CeO_2". The quantitative comparison of the integral intensities of those reflections has shown that approximately 15-20% of cerium in the modified LDH-MBT is "hidden".

Figure 2

These results demonstrate that in addition to nano-sized CeO_2, cerium is also present in amorphous (probably more soluble) forms, which is relevant for anticorrosion applications. However, the above described results do not provide any evidence about the oxidation degree of cerium cations. Therefore, an additional XPS study was performed in order to clarify the oxidation degree of Ce-based species. The survey spectrum in Figure 3 clearly demonstrates that Ce is not detectable at the very outer surface due to its coverage by the polyelectrolyte. The signal intensity for the Ce 3d region estimates that this coverage cannot have a higher thickness than approx. 5 nm which is the depth of response for the accelerate photoelectrons still to be detected.

Figure 3

The XPS Ce(3d) core level region, which was accumulated by a number of 256 scans to increase the signal-to-noise ratio, shows different states which can be described by three spin-orbit doublets as discussed in detail by Kotani and Ogasawarab.[44] According to Sharma,[45] Katta[46] and Sudarsama[47] a deconvolution of the Ce($3d_{5/2,3/2}$) was carried out and is shown in Figure 4. For Ce^{4+}($3d_{5/2}$) binding energies at 881.7 eV (a) and its satellites at 888.2 eV (a') and 897.7 eV (a'') as well as for Ce^{4+}($3d_{3/2}$) at 900.0 eV (b) and its satellites at 906.2 eV (b') and 916.1 eV (b'') can be assigned. These are characteristic for CeO_2. The peaks at 884.7 eV (c), 891.7 eV (d) and 902.4 eV (c') belong to Ce^{3+}($3d_{5/2}$) and Ce^{3+}($3d_{3/2}$) respectively.

Therefore, the XPS data confirm the existence of both oxidative states, Ce^{4+} and Ce^{3+}. From the deconvolution data a ratio Ce^{4+}/Ce^{3+} of about 3:1 can roughly be estimated. Unfortunately, the specific embedding conditions of CeO_2 nanoparticles do not admit a higher accuracy for the determination of the oxidation state ratio. The application of the mathematical functions for smoothing and fitting increase the error of the recorded raw data. Finally, the existing Ce species is best described by the formula $Ce_{x-a}O_{y-b}$.

Figure 4

The morphology and chemical compositions of LDHs were investigated by SEM-EDS analysis (Figure 5). It is clear that the Zn-rich areas correspond to LDH clusters and that sulphur (from MBT and PSS) is well visible. Contrastingly, cerium is present in small amounts. Comparing with the mapping of the samples immediately after the Ce incorporation, (**LDH_PSS(-)_Ce**), is possible to detect the signal of Ce and O presence in areas overlapping LDH particles (Figure 5e). Figure 5f depicts the EDS spectra for different LDHs. For **LDH-MBT** peaks are attributed to zinc (1.03 keV and 8.62 keV), aluminium (1.5 keV) and oxygen (0.52 keV). Also, the occurrence of a peak corresponding to sulphur at 2.32 keV is an indication of MBT being present in LDHs. After the incorporation of cerium (III) nitrate, **LDH_P(-)_Ce**, additional peaks associated with cerium occur (4.85 keV and 5.3 keV). These are an indication of the successful incorporation of cerium in modified LDH particles, which is in agreement with XRD and XPS data previously presented. Besides, cerium-based compounds were not removed by the successive modification/washing processes.

Figure 5

LDH platelets modified with polyelectrolytes were characterized by zeta potential measurements (Table 1). Initially, LDHs loaded with MBT shows zeta potential values around +30 mV. After the first modification with negatively-charged polyelectrolyte (PSS), the zeta potential decreases to ~+10 mV. The still positive value observed after deposition with PSS may be related to heterogeneities arising from charge distribution on the LDH platelets,[48, 49] which possibly limits the full coverage of LDHs with PSS. The incomplete coverage may also explain why LDH kept their anion-exchange ability in subsequent steps namely releasing MBT and taking up NO_3^- (recall XRD data). The second modification involved the incorporation of a cationic inhibitor from $Ce(NO_3)_3$ solution. In spite of the overall positive charge of LDHs modified with the first layer of PSS, one admits that locally the charge where PSS is effectively adsorbed becomes negative, which allows the deposition of Ce^{3+}. The structural and compositional analysis presented in Figures 2 and 5, supports this assumption. The treatment in $Ce(NO_3)_3$ solution led to an increase of zeta potential values up to ~+30 mV. This can be partially ascribed to formation of cerium oxide nanoparticles adsorbed on the PSS layer, which is also consistent with zeta potential measurements reported in the literature (~+37mV).[50] A second layer of PSS was deposited afterwards to cover cerium-containing species. This modification imparted a change in the zeta potential towards negative values (~-21 mV).

The final modification involved a positively-charged polyelectrolyte, PAH, with the purpose of reinforcing the shell around the particles and providing additional control over the release of Ce^{3+}, by increasing the thickness of polymeric layer covering cerium–based species. A second aim of modification with PAH was the change of zeta potential towards positive values, similar to unmodified LDHs. In this case, the zeta potential became positive (~+23 mV).

Table 1

3.2. Inhibitor release studies. LDH nanostructured materials are able to release intercalated anions by ion-exchange.[23, 33] In this section, the effect of modification of LDHs with polyelectrolytes on the release of MBT was investigated. The total loading content of LDH loaded with MBT was calculated by complete dissolution of LDHs in an acidic solution, giving values around 38 wt. % for unmodified **LDH-MBT** and around 8 wt. % for **LDH-Mod**, less than 25%. The difference in inhibitor content has to be analysed taking into account that the modified particles are heavier than LDHs without modification, due to the introduction of several layers of polyelectrolyte and addition of cerium (III) nitrate, and that the occurrence ion-exchange with nitrates in the first modification step with PSS leads to a decrease in the MBT loading content.

Figure 6 shows the release of MBT from LDHs under different conditions, namely presence of NaCl and different pH values. The release of MBT from LDHs is expected to occur mostly by ion-exchange. Indeed, the largest extent of release of MBT from **LDH-MBT** occurs in 50 mM NaCl. The modification of LDHs with different polyelectrolyte layers changes dramatically the release profile. The concentration of released MBT from **LDH-Mod** in 50 mM NaCl is more than two orders of magnitude smaller than for **LDH-MBT**, which may be explained by a combination of two factors. The first is the decrease of MBT content in **LDH-Mod** as a result of the LbL process. The second is that the presence of polyelectrolyte layers restrict the release of MBT^- under neutral conditions.

At the same time, the amount of MBT released from **LDH-Mod** depends on pH, being preferentially released under alkaline conditions. This is a relevant point as the main triggering conditions for **LDH-MBT** is the presence of NaCl, whereas in the case of **LDH-**

Mod pH is the preferential trigger. This behaviour can be explained by the pH-dependent permeability of the polyelectrolyte layers covering the LDHs.[51, 52]

Figure 6

3.3. Electrochemical studies

The inhibition provided to aluminium alloy by **LDH-Mod** was investigated by EIS. From the XRD data and release studies, the modification of LDHs with polyelectrolyte layers causes a significant decrease in the amount of MBT released and also imparts a pH-dependent release. The EIS spectra obtained on bare AA2024 after 4 hours of immersion in 50 mM NaCl solution are presented in Figure 7. This study was performed for different systems, as indicated in table 2: **LDH-MBT**, **LDH-Mod**, LDHs without corrosion inhibitors (**LDH-NO_3**), LDH-NO_3 modified with LbL containing Ce^{3+} (**LDH-NO_3-Mod**), LDH-NO_3 and LDH-MBT modified with LbL without Ce^{3+} (**LDH-NO_3-LbL** and **LDH-MBT-LbL**, respectively). Details of synthesis are available in the Electronic Supplementary Information.

Table 2

From the inspection of the impedance magnitude at low frequencies the best system is **LDH-Mod**, followed by **LDH-MBT-LbL**. The systems **LDH-NO_3-LbL**, **LDH-MBT**, **LDH-NO_3-Mod** and **LDH-NO_3** were still better than the reference system. In all the cases two time constants can be detected, at intermediate (10^1 Hz) and low frequencies (10^{-2}-10^{-1} Hz). Nevertheless, their assignment is different depending on the system. In the case of **LDH-Mod** and **LDH-MBT-LbL** the time constant at intermediate frequencies can be assigned to

the response of the native aluminium oxide, while the time constant at low frequencies is associated the corrosion processes and can be described by a charge-transfer resistance connected in parallel to the double layer capacitance. **LDH-Mod** shows the highest oxide resistance (R_{ox} 2.46 x 10^5 Ω cm^2), an indication of the protective effect rendered by these modified LDHs. In the presence of the other types of LDHs the progress of corrosion is more accentuated and the oxide response is no longer detected. Thus, the two time constants detected are ascribed to corrosion processes at the metal/solution interface (10^1 Hz) and mass-transport controlled processes (10^{-2}-10^{-1} Hz). For more details on fittings see the Electronic Supplementary Information.

The inhibition efficiency (IE) was calculated considering that R_{ct} obtained by EIS, is inversely proportional to the corrosion rate.[53, 54] Using R_{ct} values obtained by fitting of EIS spectra available in the supplementary information (Table S1) and applying the equation (1), inhibition efficiencies were obtained (Table 2):

$$IE(\%) = \left(1 - \frac{R_{ct_0}}{R_{ct}}\right) \times 100 \quad (1)$$

where R_{ct0} is the charge transfer resistance in the corrosive medium and R_{ct} is the charge transfer resistance in the inhibiting medium.

LDH loaded with MBT, shows higher IE comparing with **LDH-NO_3** (62.93% vs. 55.38%). Upon surface modification with polyelectrolytes the IE increased dramatically. For **LDH-NO_3-LbL** and **LDH-NO_3-Mod** IE values are 90.97% and 80.56%, respectively. However, the best inhibition efficiencies were found for **LDH-MBT-LbL** and **LDH-Mod**, with IE values higher than 96%.

Although **LDH-MBT-LbL** showed slightly higher inhibiting efficiency than **LDH-Mod** (calculated from the R_{ct}), the highest oxide resistance observed for **LDH-Mod** has also to be considered when we refer to the corrosion protection of aluminium alloys. In addition to high R_{ct} due to the presence of organic inhibitor MBT, the presence of Ce-based species in **LDH-**

Mod has a positive effect in increasing the oxide stability of the aluminium substrate. Therefore, the combination of both inhibitors in **LDH-Mod** contributes for the highest impedance measured among the studied systems.

From this study some important points can be highlighted. The combination of MBT and cerium-based compounds indeed impart additional protection to AA2024, when compared to individual systems. At the same time, the use of polyelectrolyte shells has a positive effect on the performance of LDHs, possible due to higher control over the release of intercalated species and reduction of alkalinisation effect associated to the presence of LDHs, as discussed by Poznyak and colleagues.[31]

Figure 7

The effect Ce^{3+} and MBT on AA2024 was investigated by DC polarization (Figure 8). The aim of this study was to rationalize the positive effect found in the EIS studies by combining Ce^{3+} and MBT. DC polarization measurements were carried out in the potential range from -1.2 V to -0.3 V, with the cathodic and anodic branches being measured separately, starting each measurement beyond the OCP. The samples were immersed during 1 hour at open circuit potential in 50 mM NaCl, 50 mM NaCl with 5 mM $Ce(NO_3)_3$, 50 mM NaCl with 2 mM MBT, and 50 mM NaCl with a mixture of 5 mM $Ce(NO_3)_3$/2 mM MBT.

In NaCl solution only, the cathodic branch is characterized by a plateau associated with diffusion-limited oxygen reduction, for potentials below -0.55 V vs. SCE (Figure 8). For more negative potentials the increase in current is associated with hydrogen reduction, which starts to dominate. In the anodic branch the current increases continuously up to 1 mA cm^{-2} at -0.3 V vs. SCE.

Ce^{3+} is a widely known inhibitor for AA2024 as reported in number of papers[55-59] and its main action consists of precipitation in places where the oxygen reduction occurs. Looking at the cathodic and anodic branches, Ce^{3+} is more effective at low polarization levels in either direction, which is consistent with deposition of cerium hydroxides on the S-phase intermetallics.[60] The current density is lower in the cathodic branch down to ca. -0.8 V when compared to the inhibitor-free electrolyte solution. Similarly, the decrease in anodic current density is considerable in the anodic polarization curve up to -0.4 V vs. SCE. The anodic current at low polarization is ascribed to the dissolution of magnesium and aluminium from S-phase and this process is also reduced as a result of precipitation of Ce oxides and hydroxides (Figure 8).

On the other hand, 2-mercaptobenzothiazole is an organic inhibitor with high efficiency towards AA2024.[30] It forms a protective film on the surface of the alloy, thereby decreasing the rate of the anodic reaction. Additionally, the high propensity of thiol-based compounds to bind Cu, can explain the effect of MBT in hampering the reduction reactions as well. MBT deposits on copper-rich intermetallics, thereby decreasing both anodic and cathodic activities occurring at these sites. In this work, MBT-containing solutions were found to cause a decrease in cathodic current, which is around one order of magnitude lower than the reference (Figure 8). Moreover, in the presence of MBT the curve associated with anodic polarization can be split into different sections. The first, at low polarization, is assigned to the dissolution of S-phase intermetallics. The second is characterized by a current-stabilizing region and the third section, at higher polarization levels, is related to intergranular corrosion.[35]

Analysing in a comparative way the different systems, all specimens immersed in solutions containing inhibitors show values of open circuit potential more positive (nobler) than AA2024 in 50 mM NaCl: E_{oc}(reference)<E_{oc}(Ce)<E_{oc}(Ce+MBT)<E_{oc}(MBT). In the presence

of MBT and MBT+Ce the cathodic current density decreases around one order of magnitude throughout the whole cathodic range sampled. At -0.8V vs. SCE current densities were 0.1 μA cm^{-2} for MBT, 0.5 μA cm^{-2} for Ce+MBT, and 10 μA cm^{-2} for Ce and for the reference system.

Additionally, the current density of the anodic branch is lower for the inhibited systems (less than 1 μA cm^{-2} at -0.45V vs. SCE) when compared to the reference (10 μA cm^{-2} at -0.45V vs. SCE). More relevant, is that the decrease in current density is the most significant in the anodic branch for Ce^{3+} + MBT (≈0.05 μA cm^{-2} at -0.45V vs. SCE). This may be associated with the combination of these species into some sort of mixed protective film deposited on the aluminium matrix which can be more stable than each inhibitor alone.

Figure 8

From the results above presented the combination of Ce+MBT seems to have a more beneficial role in the stability of the aluminium matrix, than MBT or Ce^{3+} alone, which is in agreement with EIS data presented in Figure 7. In a previous work done by our group,[23] LDH loaded with vanadate and LDH loaded with MBT were added to a 50 mM NaCl solution in bare AA2024, and analysed by EIS. The results showed a good synergetic effect with higher impedance values at lower frequencies for combined nanocontainers when compared to each LDH-inhibitor system alone. The same was observed for the combination of LDH loaded with vanadates and LDH loaded with phosphates. Taking into account that the results presented in reference [23] were obtained under similar experimental conditions, some comparisons can be done with the findings presented in this work. Looking at the EIS data, the impedance magnitude at low frequencies obtained in reference [23] is larger than the one obtained for the equivalent mass of **LDH-Mod**. This may be due to the fact that vanadates

together with MBT (or phosphates) display, as corrosion inhibitors dispersed in solution, synergistic effects towards AA2024. Nevertheless, several works available in the literature suggest that rather than the combination of different inhibitors only, other factors such as inhibitor concentration and pH play a relevant role on whether synergistic and antagonist effects can be found.[61] In this particular study, there was a significant reduction of loading content of MBT after the first modification with PSS, which may be a determining factor that limits the overall performance of **LDH-Mod**. In addition, the triggering conditions and extent of release of inhibitors is different and can also contribute for the level of inhibiting efficiency observed.

There are, however, other works that support the positive effect in combining Ce and MBT inhibitors. In the work of Montemor et al[12] cerium molybdate hollow nanospheres loaded with MBT were combined with MBT-loaded LDH and found to provide protection to galvanized steel when incorporated into a model epoxy-based coating. In another work by Kartsonakis and colleagues[65] cerium molybdate hollow nanospheres loaded with MBT were incorporated into a coating system for protection of AA2024. However, a direct comparison with our work is not possible because electrochemical data for the nanomaterials tested directly in solution are not available.

3.4. Coating performance. The modification of LDHs, aiming at creation of an outer shell that works as a reservoir layer for Ce^{3+}, may also significantly influence coating/particle interactions. A coating was used as model system to assess how this modification of LDHs reflects upon the anticorrosion behaviour provided by a protective coating layer. The selected system was a hybrid sol-gel prepared as described in the experimental section.

The direct addition of corrosion inhibitors to protective coatings was already studied in detail in previous works, including those from our group.[4, 62, 63] The direct addition of Ce^{3+} to

a hybrid sol-gel matrix was found to decrease the barrier properties of the coating system when compared to the unmodified coating.[63, 64] Similarly, the direct addition of azole-based corrosion inhibitors into coating formulations,[63, 65] leads to loss of coating protective properties when compared to the bare coating. Therefore, the isolation of Ce^{3+} and MBT from direct contact with coating matrices is necessary to avoid loss of intrinsic coating barrier properties.

Figure 9a and b depicts EIS spectra obtained on AA2024 substrates coated with a sol-gel coating (SG), whereupon **LDH-MBT** and **LDH-Mod** were added. After 4h of immersion in 500 mM NaCl (a), only one time constant is observed, attributed to the coating response. The impedance magnitude at low frequency can be ranked as follows: |Z|(SG_LDH-MBT)<|Z|(SG)<|Z|(SG_LDH-Mod). The difference in this case is associated with variation of barrier properties of the obtained coatings since the coating capacitance of all the films is nearly equal. After 5 days of immersion the difference is clear. The sol-gel coating with **LDH-Mod** shows the best performance, revealing the highest impedance magnitude at low frequencies and only one time constant (coating response). The other two sol-gel coating systems show three time constants, associated with the coating response (10^4 -10^3 Hz), oxide response (10^1 Hz), and starting electrochemical activity (10^{-2} Hz). The coating with unmodified **LDH-MBT** seems to have lower barrier properties than the non-pigmented sol-gel. This may be due to the detrimental interaction of MBT with the sol-gel matrix, possibly released at an early stage of coating preparation. However, the stability of the oxide is significantly improved and the corrosion onset is delayed.[4, 62]

Figure 9

Figure 9c presents EDS analysis for different sol-gel coatings. In the case of sol-gel coating without LDHs, only elements originated from the sol-gel and the AA2024 are detected: Ti (4.53 and 4.95 keV), Si (1.75 keV), Al (1.49 keV) and O (0.51 keV). Sol-gel coatings loaded with **LDH-MBT**, in addition to the above referred elements, also show peaks attributed to the LDH-MBT: Zn (1.04 and 8.61 keV) and S (2.33 keV). For the modified particles one extra peak can be assigned to the successfully incorporated cerium, Ce (4.87 keV). An interesting feature is observed for coatings with LDH after the immersion tests in 500 mM NaCl solution. The EDS map reveals the presence of chlorides (Cl, 2.63 keV) in the areas where LDHs are concentrated (Figure 9d), possibly as a result of ion exchange with MBT (d). This entrapment ability associated with LDHs has been described in a previous work and contributes significantly to the protection of substrates.[33]

4. Conclusions

This work reports the synthesis of layered double hydroxides with two corrosion inhibitors, 2-mercaptobenzothiazole (in anionic form) and cerium (III) nitrate. The first was intercalated by ion-exchange, whereas the second was incorporated by Layer-by-Layer (LbL) method, between polyelectrolyte layers adsorbed on LDH nanoplatelets.

The structural and compositional data showed that layered double hydroxides behave as a dynamic system during the LbL process, exchanging part of the anionic inhibitor previously intercalated with species available in cerium- and polyelectrolyte-containing aqueous solutions. Furthermore, cerium was incorporated in the nanocontainers, both as nano-sized crystalline CeO_2 as well as in amorphous forms.

The modification of LDHs with polyelectrolytes changes the main triggering conditions of release of inhibitors intercalated within layered double hydroxides, from exchange with aggressive species (NaCl) to pH changes (spectrophotometric data).

In spite of partial loss of 2-mercaptobenzothiazole during the LbL process, layered double hydroxides modified with cerium and polyelectrolytes were found to protect aluminium alloy 2024 in NaCl solution for long immersion times, which was rationalized by the formation of inhibiting layer on the aluminium substrate combining both cerium and the organic inhibitor. However, there is still space for improving inhibitor loading content in future works. One possibility is to perform the modification of LDHs with PSS in a solution saturated with 2-mercaptobenzothiazole, thereby preventing the release of inhibitor.

The addition of modified layered double hydroxides to sol-gel formulations was found to impart the highest barrier properties and active corrosion protection. These results open prospects for development of smart-coatings based on nanocontainers with dual release of active species, to enhance a specific functionality or combine different functionalities.

Acknowledgements:

This work was developed in the scope of the project CICECO-Aveiro Institute of Materials (Ref. FCT UID /CTM /50011/2013), financed by national funds through the FCT/MEC and when applicable co-financed by FEDER under the PT2020 Partnership Agreement. This work is also funded by ERDF Funds through Operational Competitiveness Programme – COMPETE in the frame of the project FUNACOP – FCOMP-01-0124-FEDER- 38777. JT thanks FCT for researcher grant IF/00347/2013. The authors thank Dr. Kiryl Yasakau for the support on the synthesis of sol-gel coatings.

Electronic Supplementary Information: Modification of layered double hydroxides with polyelectrolytes in the absence of cerium (III) nitrate and fitting of EIS data depicted in Figure 7.

References:

1. D. Raps, T. Hack, M. Kolb, M. L. Zheludkevich and O. Nuyken, in *Smart Coatings Iii*, eds. J. Baghdachi and T. Provder, 2010, vol. 1050, pp. 165-189.
2. D. Borisova, H. Moehwald and D. G. Shchukin, *Acs Nano*, 2011, **5**, 1939-1946.
3. D. Borisova, H. Moehwald and D. G. Shchukin, *ACS Appl. Mater. Interfaces*, 2012, **4**, 2931-2939.
4. F. Maia, J. Tedim, A. D. Lisenkov, A. N. Salak, M. L. Zheludkevich and M. G. S. Ferreira, *Nanoscale*, 2012, **4**, 1287-1298.
5. N. Wang, K. Cheng, H. Wu, C. Wang, Q. Wang and F. Wang, *Prog. Org. Coat.*, 2012, **75**, 386-391.
6. A. Joshi, E. Abdullayev, A. Vasiliev, O. Volkova and Y. Lvov, *Langmuir*, 2013, **29**, 7439-7448.
7. Y. M. Lvov, D. G. Shchukin, H. Möhwald and R. R. Price, *Acs Nano*, 2008, **2**, 814-820.
8. D. Snihirova, L. Liphardt, G. Grundmeier and F. Montemor, *J. Solid State Electrochem.*, 2013, **17**, 2183-2192.
9. N. Granizo, J. M. Vega, D. de la Fuente, B. Chico and M. Morcillo, *Prog. Org. Coat.*, 2013, **76**, 411-424.
10. T. T. X. Hang, T. A. Truc, N. T. Duong, N. Pébère and M.-G. Olivier, *Prog. Org. Coat.*, 2012, **74**, 343-348.
11. D. Li, F. Wang, X. Yu, J. Wang, Q. Liu, P. Yang, Y. He, Y. Wang and M. Zhang, *Prog. Org. Coat.*, 2011, **71**, 302-309.
12. M. F. Montemor, D. V. Snihirova, M. G. Taryba, S. V. Lamaka, I. A. Kartsonakis, A. C. Balaskas, G. C. Kordas, J. Tedim, A. Kuznetsova, M. L. Zheludkevich and M. G. S. Ferreira, *Electrochim. Acta*, 2012, **60**, 31-40.
13. S. P. V. Mahajanarn and R. G. Buchheit, *Corrosion*, 2008, **64**, 230-240.

14. X. Yu, J. Wang, M. Zhang, P. Yang, L. Yang, D. Cao and J. Li, *Solid State Sci.*, 2009, **11**, 376-381.

15. S. P. Newman and W. Jones, *New J. Chem.*, 1998, **22**, 105-115.

16. R. B. Leggat, W. Zhang, R. G. Buchheit and S. R. Taylor, *Corrosion*, 2002, **58**, 322-328.

17. W. Zhang and R. G. Buchheit, *Corrosion*, 2002, **58**, 591-600.

18. R. G. Buchheit, S. B. Mamidipally, P. Schmutz and H. Guan, *Corrosion*, 2002, **58**, 3-14.

19. F. Zhang, L. Zhao, H. Chen, S. Xu, D. G. Evans and X. Duan, *Angew. Chem. Int. Ed.*, 2008, **47**, 2466-2469.

20. J.-Y. Uan, J.-K. Lin and Y.-S. Tung, *J. Mater. Chem.*, 2010, **20**, 761-766.

21. J. Tedim, M. L. Zheludkevich, A. N. Salak, A. Lisenkov and M. G. S. Ferreira, *J. Mater. Chem.*, 2011, **21**, 15464-15470.

22. J. Tedim, M. L. Zheludkevich, A. C. Bastos, A. N. Salak, A. D. Lisenkov and M. G. S. Ferreira, *Electrochim. Acta*, 2014, **117**, 164-171.

23. J. Tedim, S. K. Poznyak, A. Kuznetsova, D. Raps, T. Hack, M. L. Zheludkevich and M. G. S. Ferreira, *ACS Appl. Mater. Interfaces*, 2010, **2**, 1528-1535.

24. N. B. D. Ho, J.C. Scully, T. Markley, M. Forsyth, B. Hinton, *J. Electrochem. Soc.*, 2006, **153**, B392-B401.

25. N. Birbilis, R. G. Buchheit, D. L. Ho and M. Forsyth, *Electrochem. Solid-State Lett.*, 2005, **8**, C180-C183.

26. S. Kallip, A. C. Bastos, K. A. Yasakau, M. L. Zheludkevich and M. G. S. Ferreira, *Electrochem. Commun.*, 2012, **20**, 101-104.

27. E. L. Ferrer, A. P. Rollon, H. D. Mendoza, U. Lafont and S. J. Garcia, *Microporous Mesoporous Mater.*, 2014, **188**, 8-15.

28. S. V. Lamaka, D. G. Shchukin, D. V. Andreeva, M. L. Zheludkevich, H. Möhwald and M. G. S. Ferreira, *Adv. Funct. Mater.*, 2008, **18**, 3137-3147.

29. D. G. Shchukin, S. V. Lamaka, K. A. Yasakau, M. L. Zheludkevich, M. G. S. Ferreira and H. Mohwald, *J. Phys. Chem. C*, 2008, **112**, 958-964.

30. M. L. Zheludkevich, K. A. Yasakau, S. K. Poznyak and M. G. S. Ferreira, *Corrosion Science*, 2005, **47**, 3368-3383.

31. S. K. Poznyak, J. Tedim, L. M. Rodrigues, A. N. Salak, M. L. Zheludkevich, L. F. P. Dick and M. G. S. Ferreira, *ACS Appl. Mater. Interfaces*, 2009, **1**, 2353-2362.

32. M. B. Bethencourt, F. J.; Calvino, J. J.; Marcos, M.; Rodriguez-Chacon, M. A., *Corros. Sci.*, 1998, **40**, 1803-1819.

33. J. Tedim, A. Kuznetsova, A. N. Salak, F. Montemor, D. Snihirova, M. Pilz, M. L. Zheludkevich and M. G. S. Ferreira, *Corros. Sci.*, 2012, **55**, 1-4.

34. K. A. Yasakau, J. Carneiro, M. L. Zheludkevich and M. G. S. Ferreira, *Surf. Coat. Technol.*, 2014, **246**, 6-16.

35. V. Guillaumin and G. Mankowski, *Corros. Sci.*, 1998, **41**, 421-438.

36. S. K. Yun and T. J. Pinnavaia, *Chem. Mater.*, 1995, **7**, 348-354.

37. J. Das, D. Das and K. M. Parida, *J. Colloid Interface Sci.*, 2006, **301**, 569-574.

38. C. Barriga, W. Jones, P. Malet, V. Rives and M. A. Ulibarri, *Inorg. Chem.*, 1998, **37**, 1812-1820.

39. A. N. Salak, J. Tedim, A. I. Kuznetsova, L. G. Vieira, J. L. Ribeiro, M. L. Zheludkevich and M. G. S. Ferreira, *J. Phys. Chem. C*, 2013, **117**, 4152-4157.

40. Q. Dai, X. Wang, G. Chen, Y. Zheng and G. Lu, *Microporous Mesoporous Mater.*, 2007, **100**, 268-275.

41. N. Nesakumar, S. Sethuraman, U. M. Krishnan and J. B. B. Rayappan, *J. Colloid Interface Sci.*, 2013, **410**, 158-164.

42. M. Chelliah, J. B. B. Rayappan and U. M. Krishnan, *J. Appl. Sci.*, 2012, **12**, 1734-1737.

43. A. N. Salak, J. Tedim, A. I. Kuznetsova, J. L. Ribeiro, L. G. Vieira, M. L. Zheludkevich and M. G. S. Ferreira, *Chem. Phys.*, 2012, **397**, 102-108.

44. A. Kotani and H. Ogasawara, *J. Electron. Spectrosc. Relat. Phenom.*, 1992, **60**, 257-299.

45. S. Sharma and M. S. Hegde, *J. Chem. Phys.*, 2009, **130**, 114706.

46. L. Katta, P. Sudarsanam, G. Thrimurthulu and B. M. Reddy, *Appl. Catal., B*, 2010, **101**, 101-108.

47. P. Sudarsanam, P. R. Selvakannan, S. K. Soni, S. K. Bhargava and B. M. Reddy, *RSC Adv.*, 2014, **4**, 43460-43469.

48. Y. Zhou, X. Sun, K. Zhong, D. G. Evans, Y. Lin and X. Duan, *Ind. Eng. Chem. Res.*, 2012, **51**, 4215-4221.

49. J. B. Swadling, J. L. Suter, H. C. Greenwell and P. V. Coveney, *Langmuir*, 2013, **29**, 1573-1583.

50. S. Patil, A. Sandberg, E. Heckert, W. Self and S. Seal, *Biomaterials*, 2007, **28**, 4600-4607.

51. K. Glinel, C. Déjugnat, M. Prevot, B. Schöler, M. Schönhoff and R. v. Klitzing, *Colloids Surf. Physicochem. Eng. Aspects*, 2007, **303**, 3-13.

52. J. A. Hiller and M. F. Rubner, *Macromolecules*, 2003, **36**, 4078-4083.

53. E. Barsoukov and J. R. Macdonal, *Impedance Spectroscopy*, Wiley Interscience, New Jersey, 2nd edn., 2005.

54. A. C. Bastos, M. L. Zheludkevich and M. G. S. Ferreira, *Port. Electrochim. Acta*, 2008, **26**, 47-54.

55. J. A. J. Aldykiewicz, A. J. Davenport and H. S. Isaacs, *J. Electrochem. Soc.*, 1996, **143**, 147-154.

56. B. Davó and J. J. de Damborenea, *Electrochim. Acta*, 2004, **49**, 4957-4965.

57. A. Aballe, M. Bethencourt, F. J. Botana and M. Marcos, *J. Alloys Compd.*, 2001, **323–324**, 855-858.

58. M. A. Arenas, M. Bethencourt, F. J. Botana, J. de Damborenea and M. Marcos, *Corros. Sci.*, 2001, **43**, 157-170.

59. B. A. Bilal and E. Z. Muller, *Z. Naturforsch., A: Phys. Sci.*, 1992, **47**, 974-984.

60. K. A. Yasakau, M. L. Zheludkevich, S. V. Lamaka and M. G. S. Ferreira, *J. Phys. Chem. B*, 2006, **110**, 5515-5528.

61. B. D. Chambers, S. R. Taylor and M. W. Kendig, *Corrosion*, 2005, **61**, 480-489.

62. M. L. Zheludkevich, D. G. Shchukin, K. A. Yasakau, H. Möhwald and M. G. S. Ferreira, *Chem. Mater.*, 2007, **19**, 402-411.

63. M. L. Zheludkevich, R. Serra, M. F. Montemor, K. A. Yasakau, I. M. M. Salvado and M. G. S. Ferreira, *Electrochim. Acta*, 2005, **51**, 208-217.

64. D. Snihirova, S. V. Lamaka and M. F. Montemor, *Electrochim. Acta*, 2012, **83**, 439-447.

65. I. A. Kartsonakis, A. C. Balaskas and G. C. Kordas, *Corros. Sci.*, 2011, **53**, 3771-3779.

FIGURE CAPTIONS

Scheme 1: Approach used in the surface modification of LDH with PSS, PAH and cerium (III) nitrate.

Table 1: Zeta potential values of LDH particles throughout the modification process.

Table 2: LDH-based systems prepared and measured by electrochemical impedance measurements with IE values of LDH-based systems estimated from charge transfer resistance.

Figure 1: XRD patterns of LDH powders before (LDH-NO_3) and after intercalation with MBT^- (LDH-MBT). Inset shows the range of (110) diffraction reflections. XRD patterns of LDH-MBT powders throughout the modification process. Diffraction peaks associated with cerium oxide phase are represented by red dots.

Figure 2: Top: XRD patterns of (1) the powder obtained as a result of calcination of LDH-MBT sample after the second modification step and (2) nano-powder of CeO_2. Bottom: diffraction peaks of CeO_2 in the XRD patterns of the mechanical mixture of LDH-MBT + nano- CeO_2 (open symbols) and the LDH-MBT sample after the second modification step (solid symbols).

Figure 3: XPS survey spectrum of LDH-MBT + nano-CeO_2.

Figure 4: XPS spectra of the Ce($3d_{5/2,3/2}$) core level region with deconvolution assigned to Ce states for determination of the Ce^{4+}/Ce^{3+} ratio.

Figure 5: SEM and EDS mapping of LDHs: (a) SEM image, (b) Zn mapping, (c) S mapping and (d) Ce mapping. Overlapping of SEM image, O mapping and Ce mapping of **LDH_PSS(-)_Ce** sample (e). EDS analysis throughout the modification process (f).

Figure 6: MBT release profiles for **LDH-MBT** and **LDH-Mod** under different conditions (λ=320 nm).

Figure 7: Bode representation of EIS spectra acquired for AA2024 bare substrates after 4 hours of immersion in 50 mM NaCl solution with: LDH loaded with NO_3 and MBT, with LbL modification and LbL modification with cerium-based compounds incorporated (Table 2). (a) impedance magnitude and (b) phase angle.

Figure 8: DC polarization curves for AA2024 samples immersed in 50 mM NaCl solution with 1 mM $Ce(NO_3)_3$, saturated solution of MBT (2 mM solution) and a mixture of both (5 mM $Ce(NO_3)_3$/2 mM MBT) after 1 hour of immersion.

Figure 9: Bode representation of EIS spectra for AA2024 coated with sol-gel, and sol-gel loaded with **LDH-MBT** and **LDH-Mod** after (a) 4 hours and (b) 5 days of immersion in a 500 mM NaCl solution. (c) EDS analysis after immersion tests of coated AA2024 sample in regions with agglomeration of LDHs, as observed in (d).

Scheme 1: Approach used in the surface modification of LDH with PSS, PAH and cerium (III) nitrate.

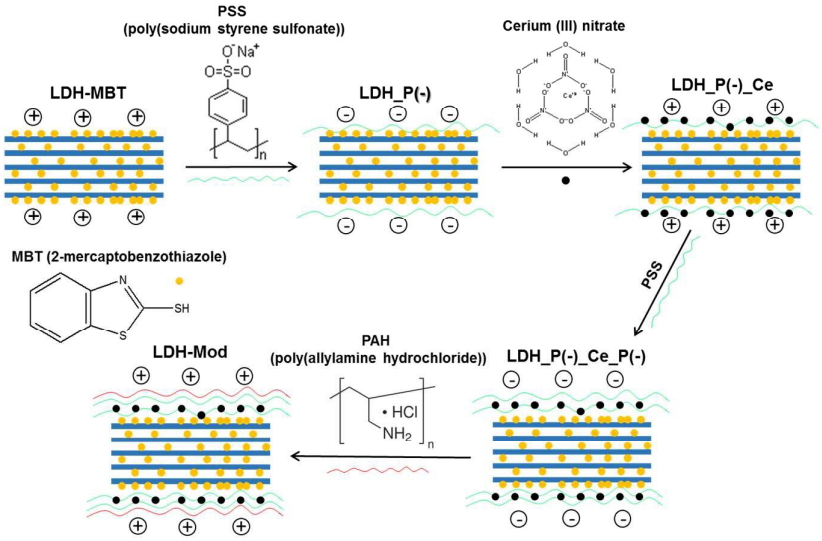

Table 1: Zeta potential values of LDH particles throughout the modification process.

Sample	LDH-MBT	LDH_P(-)	LDH_P(-)_Ce	LDH_P(-)_Ce_P(-)	LDH-Mod
Zeta potential (mV)	+31.8	+9.8	+29.5	-21.3	+22.8

Table 2: LDH-based systems prepared and used in electrochemical impedance measurements. IE values of LDH-based systems in dispersed in 50 mM NaCl in bare AA2024.

System	MBT within LDH	Surface modification with polyelectrolytes by LbL	Cerium-based species between polyelectrolyte layers	IE (%)
LDH-NO_3	No	No	No	55.38
LDH-NO_3-LbL	No	Yes	No	90.97
LDH-NO_3-Mod	No	Yes	Yes	80.56
LDH-MBT	Yes	No	No	62.93
LDH-MBT-LbL	Yes	Yes	No	96.45
LDH-Mod	Yes	Yes	Yes	96.01

Figure 1: XRD patterns of LDH powders before (LDH-NO_3) and after intercalation with MBT^- (LDH-MBT). Inset shows the range of (110) diffraction reflections. XRD patterns of LDH-MBT powders throughout the modification process. Diffraction peaks associated with cerium oxide phase are represented by red dots.

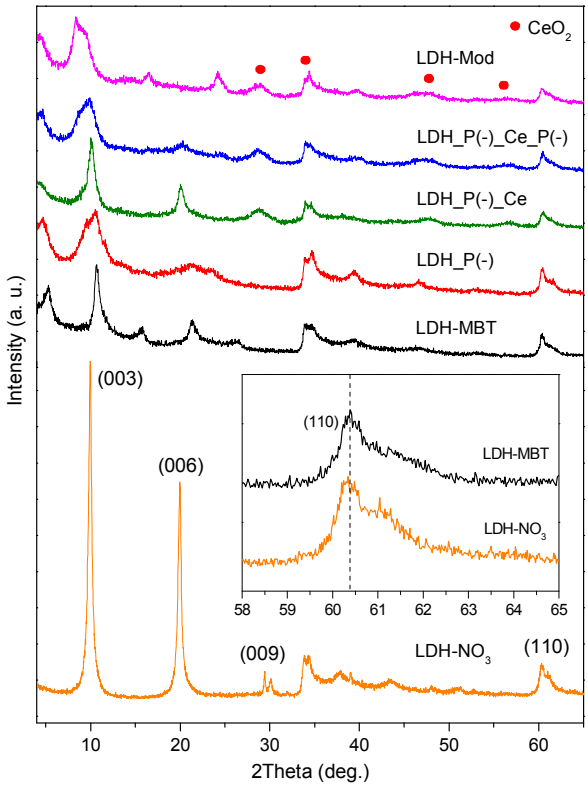

Figure 2: Top: XRD patterns of (1) the powder obtained as a result of calcination of LDH-MBT sample after the second modification step and (2) nano-powder of CeO_2. Bottom: diffraction peaks of CeO_2 in the XRD patterns of the mechanical mixture of LDH-MBT + nano- CeO_2 (open symbols) and the LDH-MBT sample after the second modification step (solid symbols).

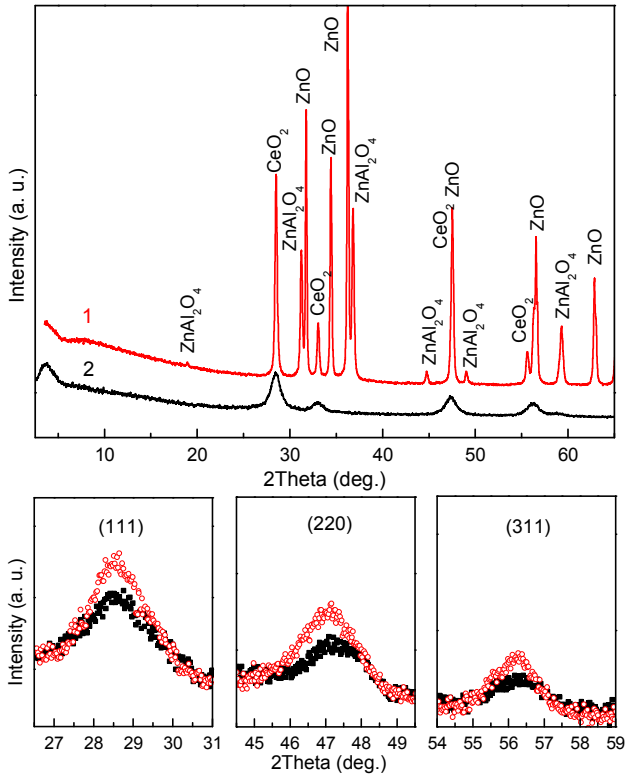

Figure 3: XPS survey spectrum of LDH-MBT + nano-CeO_2.

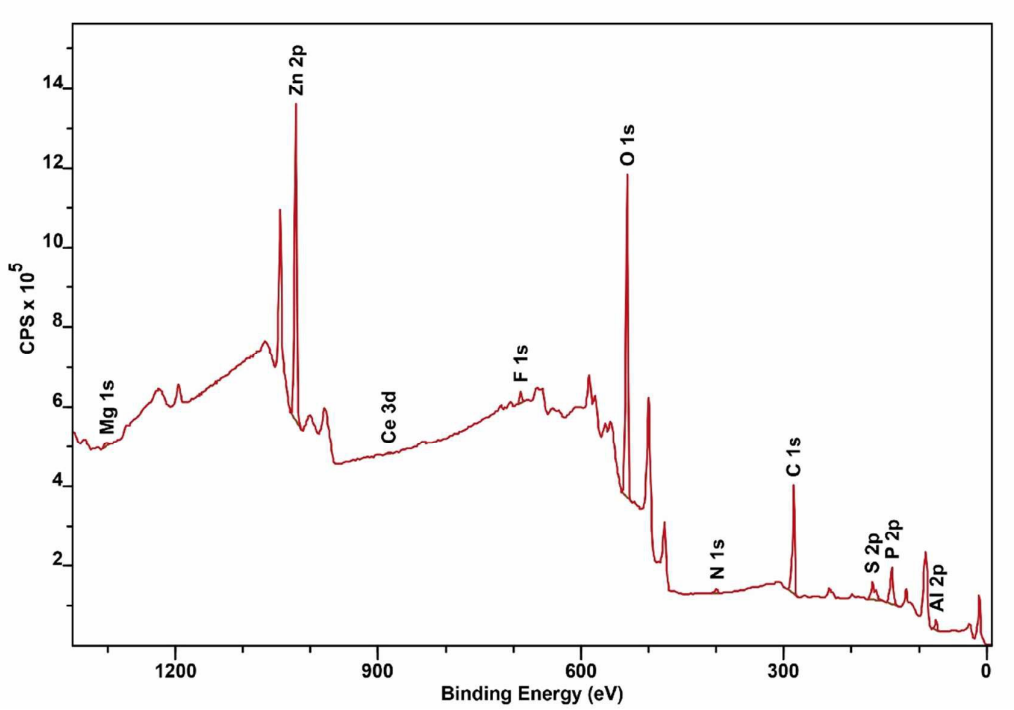

Figure 4: XPS spectra of the Ce($3d_{5/2,3/2}$) core level region with deconvolution assigned to Ce states for determination of the Ce^{4+}/Ce^{3+} ratio.

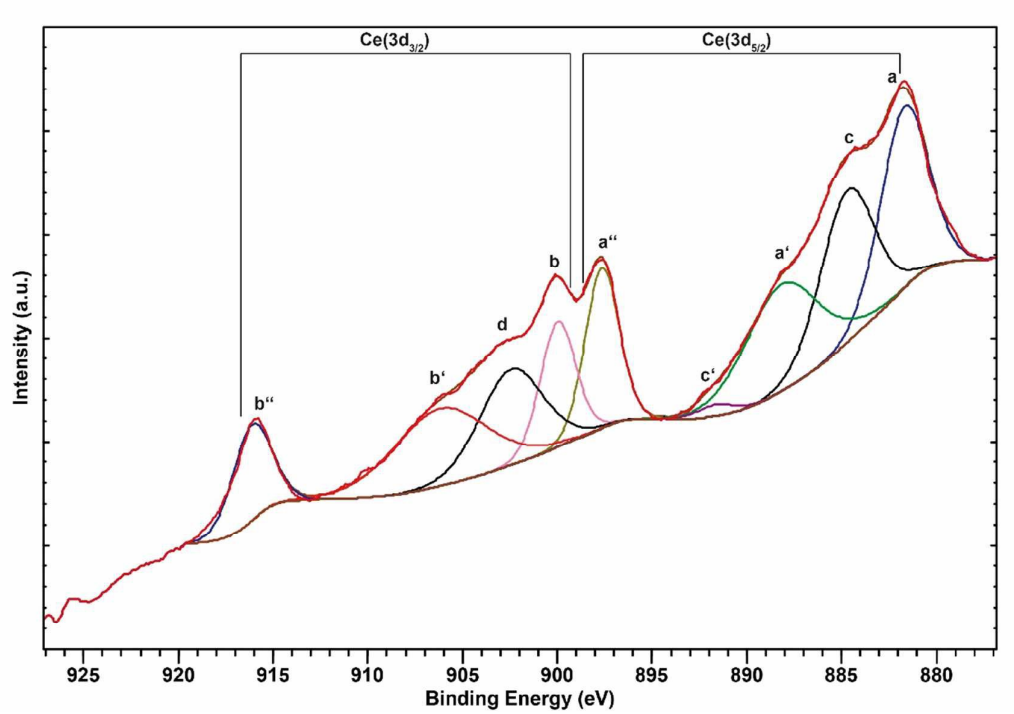

Figure 5: SEM and EDS mapping of LDHs: (a) SEM image, (b) Zn mapping, (c) S mapping and (d) Ce mapping. Overlapping of SEM image, O mapping and Ce mapping of **LDH_PSS(-)_Ce** sample (e). EDS analysis throughout the modification process (f).

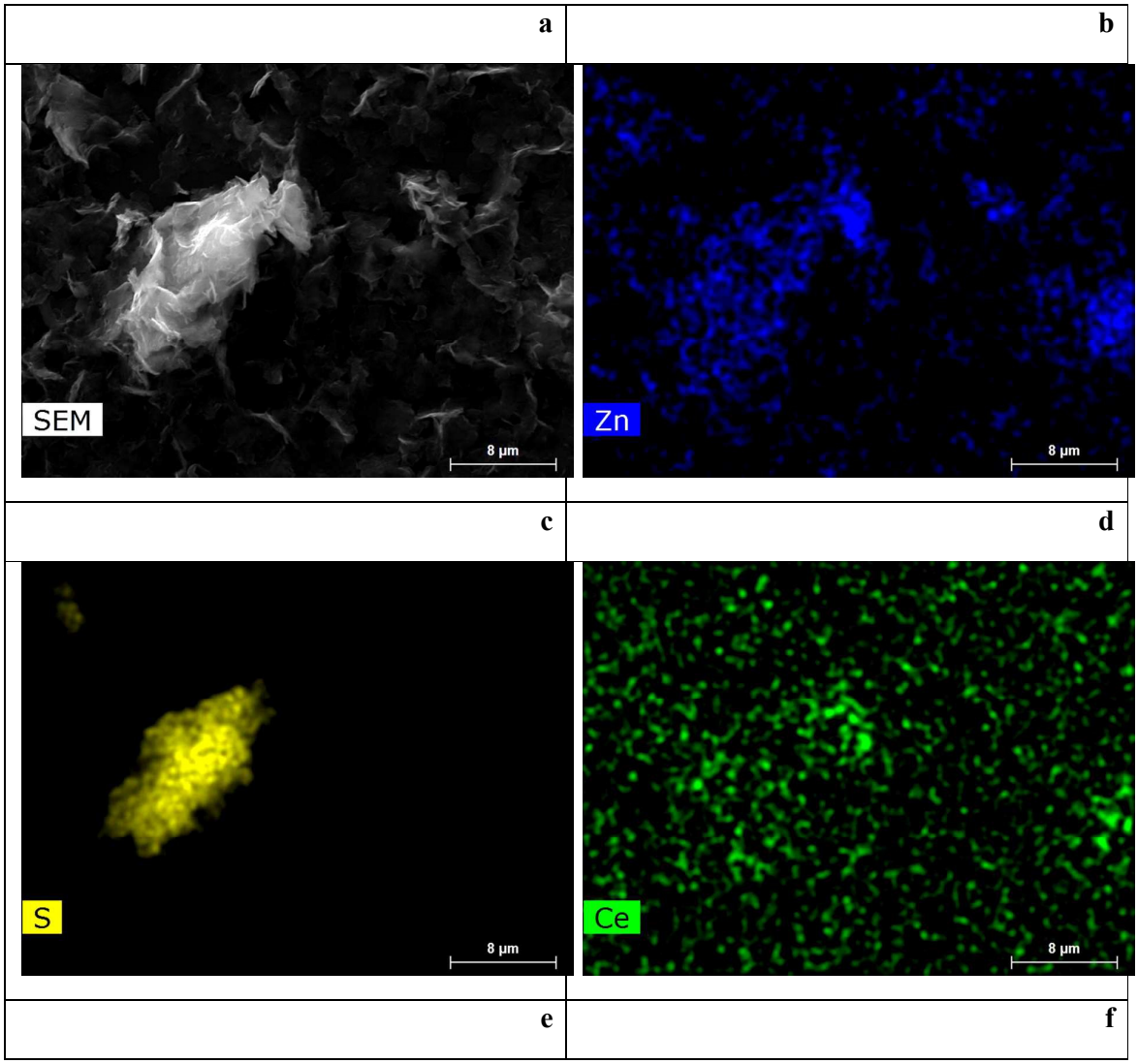

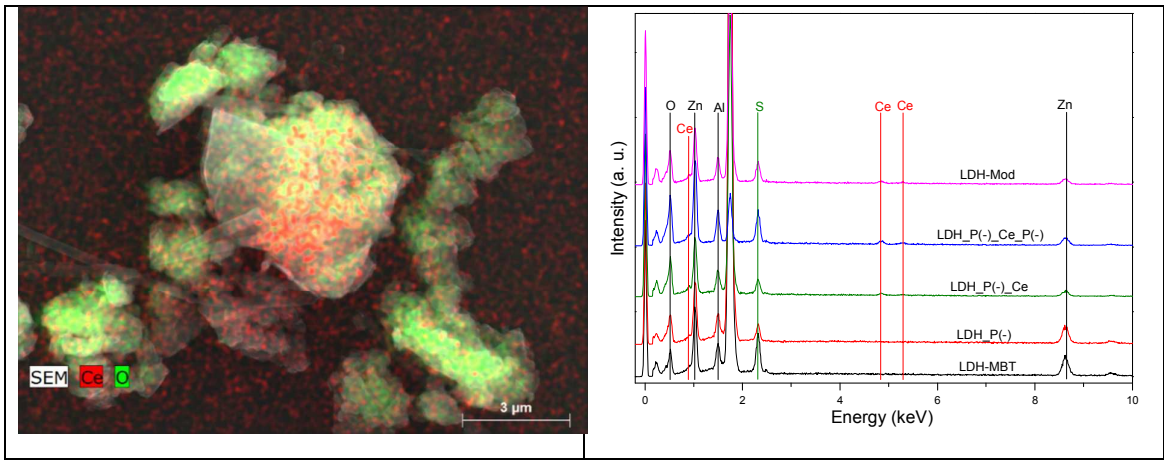

Figure 6: MBT release profiles for **LDH-MBT** and **LDH-Mod** under different conditions (λ=320 nm).

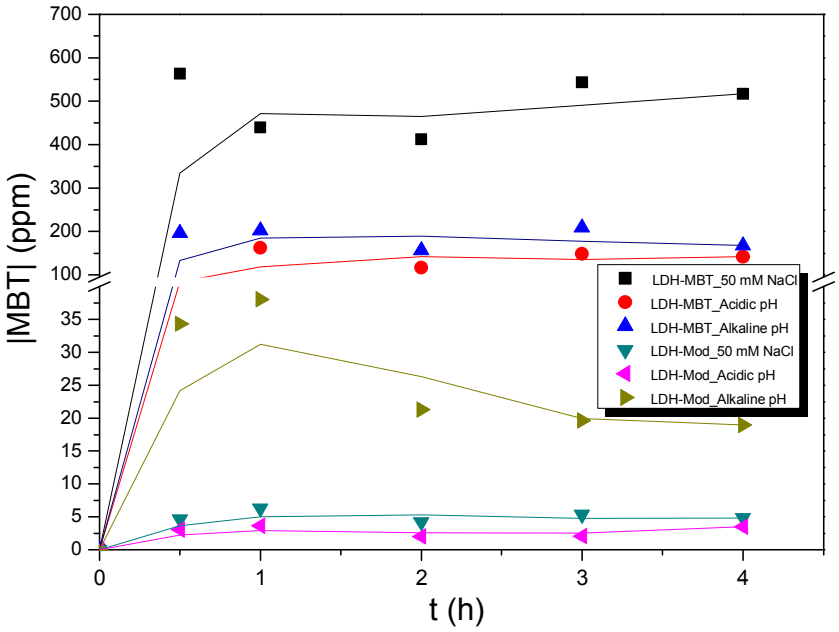

Figure 7: Bode representation of EIS spectra acquired for AA2024 bare substrates after 4 hours of immersion in 50 mM NaCl solution with: LDH loaded with NO_3 and MBT, with LbL modification and LbL modification with cerium-based compounds incorporated (Table 2). (a) impedance magnitude and (b) phase angle.

a

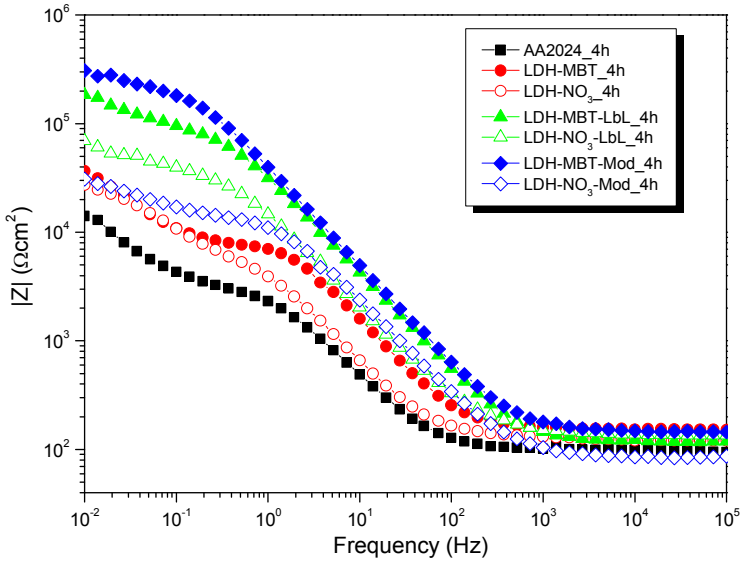

b

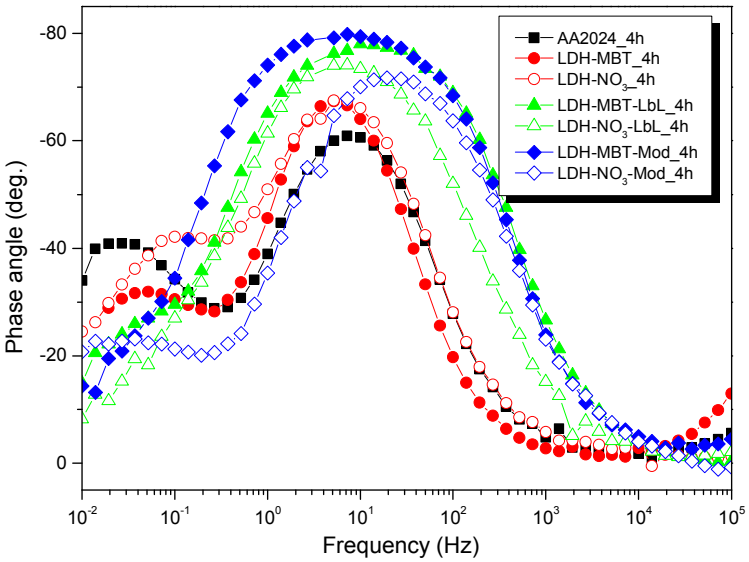

Figure 8: DC polarization curves for AA2024 samples immersed in 50 mM NaCl solution with 1 mM $Ce(NO_3)_3$, saturated solution of MBT (2 mM solution) and a mixture of both (5 mM $Ce(NO_3)_3$/2 mM MBT) after 1 hour of immersion.

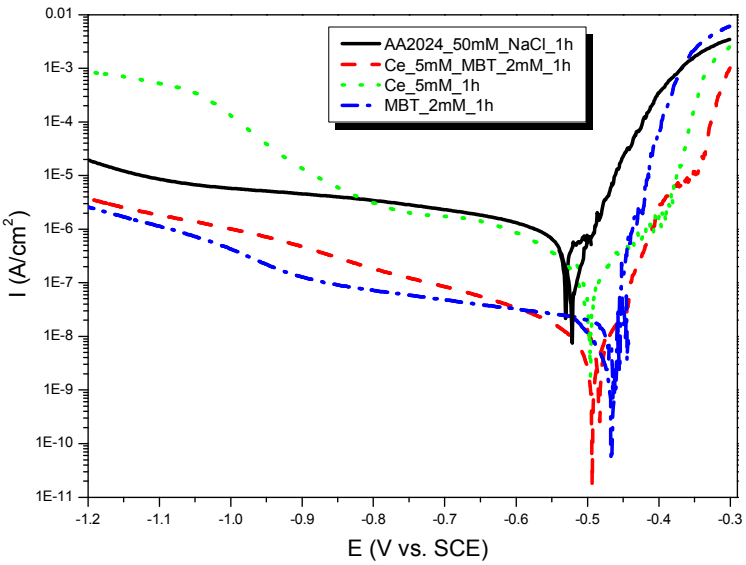

Figure 9: Bode representation of EIS spectra for AA2024 coated with sol-gel, and sol-gel loaded with **LDH-MBT** and **LDH-Mod** after (a) 4 hours and (b) 5 days of immersion in a 500 mM NaCl solution. (c) EDS analysis after immersion tests of coated AA2024 sample in regions with agglomeration of LDHs, as observed in (d).